Waves along the Equator in the Atlantic*

ELI JOEL KATZ

Lamont-Doherty Earth Observatory, Columbia University, Palisades, New York

ABSTRACT

Spectra of two hundred days of data from five inverted echo sounders deployed along the equator in 1983–84 and a thousand days of 30 crossings of the equator by the TOPEX/POSEIDON altimeter in 1993–95 are both found to have enhanced variance of sea surface displacement in two frequency bands centered nominally about 50^{-1} and 25^{-1} cycles/day. Complex empirical orthogonal function analysis of the two bands finds much of the variance being accounted for by eastward and westward propagating waves, respectively, that are coherent across the basin.

The eastward propagating wave is identifiable as a first-mode Kelvin wave with a period of 54 (49) days in the sounder (altimeter) dataset, a basinwide wavelength and a speed of 2.1 (1.8) m s^{-1}. It is suggested that the westward propagating wave is a surface expression of the meridional oscillation of the Equatorial Undercurrent about the equator, presumably induced by a tropical instability wave, with a period of 24 (28) days, a wavelength of 600 (580) km, and a speed of 0.30 (0.23) m s^{-1}. The amplitude variation with time and longitude of both waves is described and, for the Kelvin wave, compared to the zonal wind stress in the west during 1993–95.

1. Introduction

In 1983, as a part of the SEQUAL/FOCAL programs to observe an annual cycle of the upper-ocean dynamics in the equatorial Atlantic Ocean, an array of ten inverted echo sounder sites was maintained in that basin (by multiple overlapping deployments). Five sites were located directly on the equator between 34° and 1°W (Fig. 1) and simultaneously recorded hourly observations of the two-way acoustic travel time from ocean bottom to surface for 252 days. From repeated cross-correlation between one (arbitrarily chosen) site and the others, after appropriate bandpass filtering, a plot of the lag time for maximum correlation was reported (Katz 1987a, reproduced here in Fig. 1). The slope of the regression line of the lag time with longitude yielded an eastward propagation speed of 2.35 ($\pm$0.22) m s^{-1}, which was identified as an appropriate speed for the first baroclinic mode as computed theoretically from average equatorial density profiles. The existence of several years of TOPEX/POSEIDON altimetric data encompassing this same region allows for an extended study of these Kelvin waves.

A second, frequently observed, equatorial wave phenomenon is the so-called tropical instability wave (TIW). The most striking early evidence of its existence came from satellite sea surface temperature images in the Pacific (Legekis 1977) and theoretical studies, beginning with Philander[1] (1976) and extending to the present time (e.g., Proehl 1996), have related the phenomenon to an instability of the strong zonal flows that characterize the circulation in all three equatorial oceans.

Qiao and Weisberg (1995) present a tabular summary of 21 observations of TIWs from velocity, sea surface temperature, and sea level measurements in the Atlantic and Pacific Oceans. The reported estimates of its period, wavelength, and phase speed vary widely (each by a factor of almost 10), but they conclude that the observations "generally show westward propagating waves with period, zonal wavelength and phase speed centered about 3 weeks, 1000 km and -50 cm s^{-1}, respectively." The presence of this wave in the echo sounder data was not previously reported but it will now be demonstrated in both the sounder and altimetry data.

2. Spectral analysis

a. Inverted echo sounders

Spectral analyses of the energy density of the measured acoustic travel time averaged over five frequency

---

Corresponding author address: Dr. Eli Joel Katz, Lamont-Doherty Earth Observatory, Columbia University, Palisades, NY 10964. E-mail: ejk@ldeo.columbia.edu

[1] Who was motivated by the more tentative observation resulting from the GATE program in the Atlantic (reported by Düing et al. 1975).
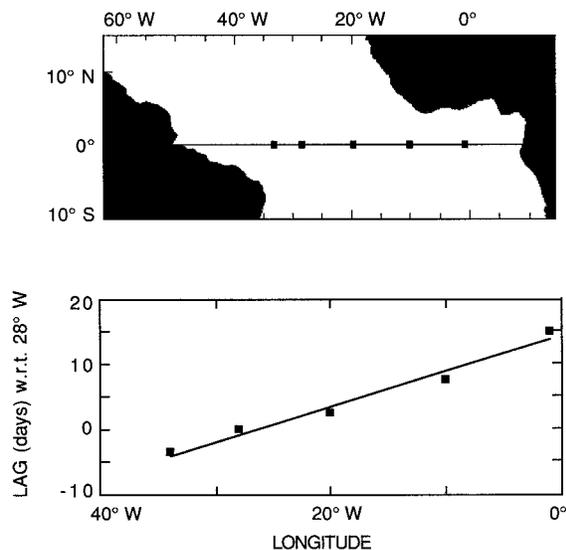
FIG. 1. The location of five inverted echo sounders deployed along the equator in 1983–84 (upper panel) and the lag time for maximum cross correlation between the sounder at 28°W and the others (lower panel) (reproduced from Katz 1987a).

bands are shown in Fig. 2. The left-hand panel is from the sounders deployed at 0°, 10° W, which yielded the longest continuous record of 886 days and is typical of all the sites. As indicated in the figure, the sounder clearly resolves the baroclinic inertia–gravity wave field (e.g., Garzoli and Katz 1981) and various barotropic tidal frequencies (Cartwright 1982). It suggests the presence of waves at frequencies lower than the inertia–gravity waves, but not at the 95% confidence limit as shown.

The second panel in Fig. 2 is the result of averaging the spectral density of a single frequency band for the five sounders located on the equator during the 252 days that they were sampled simultaneously. The averaging at different locations changes the spectral density of the tidal amplitudes as they vary geographically and the bandwidth has changed; and inertia–gravity wave densities are diffused as their frequency vary with the vertical density profile of the site. However, two lower frequency signals not well resolved in the spectrum from a single site are now statistically significant at a 95% confidence limit.

The two peaks of energy density (centered at periods of 50 and 23 days), suggest low-frequency motion common to all or most of the array at frequencies greater than seasonal. Their dominance of the variance at periods greater than 5 days, given by the area under the curve, is shown in the insert.

b. Altimeter

Every 9.9156 days the TOPEX/Poseidon altimeter makes 30 crossings of the equator between 43° and 2°W. For this analysis, cycles 2–110 are included describing three years of observations beginning in October 1992. The sea surface height for each crossing is obtained from the MGDR records provided by NASA, with corrections applied as recommended (Benada 1993) except for the tidal model. For the latter, a newer version of the Cartwright and Ray tidal model (updated by using an analysis of the first year of the T/P altimeter data; Ray 1996, personal communication) was used to replace the tide model provided. To smooth the data a little and to collocate all the crossings, a linear regression was applied to an arc of corrected sea surface heights between 30′N and S and then interpolated to the equator [Katz et al. (1995) describe the procedure]. The result is 30 time series of 109 observations of sea surface height every 1°25′ (nominally) of longitude along the equator.

The variance-preserving plot from a spectral analysis of the 30 time series averaged over a frequency band of width (634.6^{-1} cycles day^{-1}) is shown in Fig. 3. Three bands of above-background variance are noted: a low frequency band, periods between 106 and 211 days, that describes the seasonal variance of the sea surface and apparently exceeds the interannual variance in this 3-year record and, at higher frequencies, the two bands of enhanced variance previously described by the sounder records. The altimeter centers the first band at a period between 42 or 49 days and finds the second centered at 29 days, with a hint of a second band at 23 days just before signal noise dominates.

c. Analysis

To study the two energetic frequency bands, the time series at each location along the equator were first filtered into two bands: 30–60 days and 10–30 days (for the sounders); and 3–6 cycles and 3-cycle low-pass filtered (for the altimeter). A complex empirical orthogonal function (CEOF) analysis (Horel 1984) was performed on each of the four filtered time series.

The sounder data are left in microseconds of two way acoustic travel time and raw and filtered examples of the signals were given in Katz (1987a,b). From comparisons with cotemporal hydrographic stations, Katz (1987b) derived a conversion factor of 7.89 dyn cm (0/500 db) per ms of travel time.

The altimeter provides a direct measurement of sea surface height. An example from one typical pass of the raw time series and the results of filtering are shown in Fig. 4. In the upper panel the result of removing several tidal alias frequencies is shown to be quite negligible (thicker line compared to thin line), giving confidence that the tidal model has adequately removed the tidal signals from the dataset. The lower panel shows that the amplitude in both frequency bands is of an order of magnitude of a few centimeters, compared to the annual signal of 20 cm.
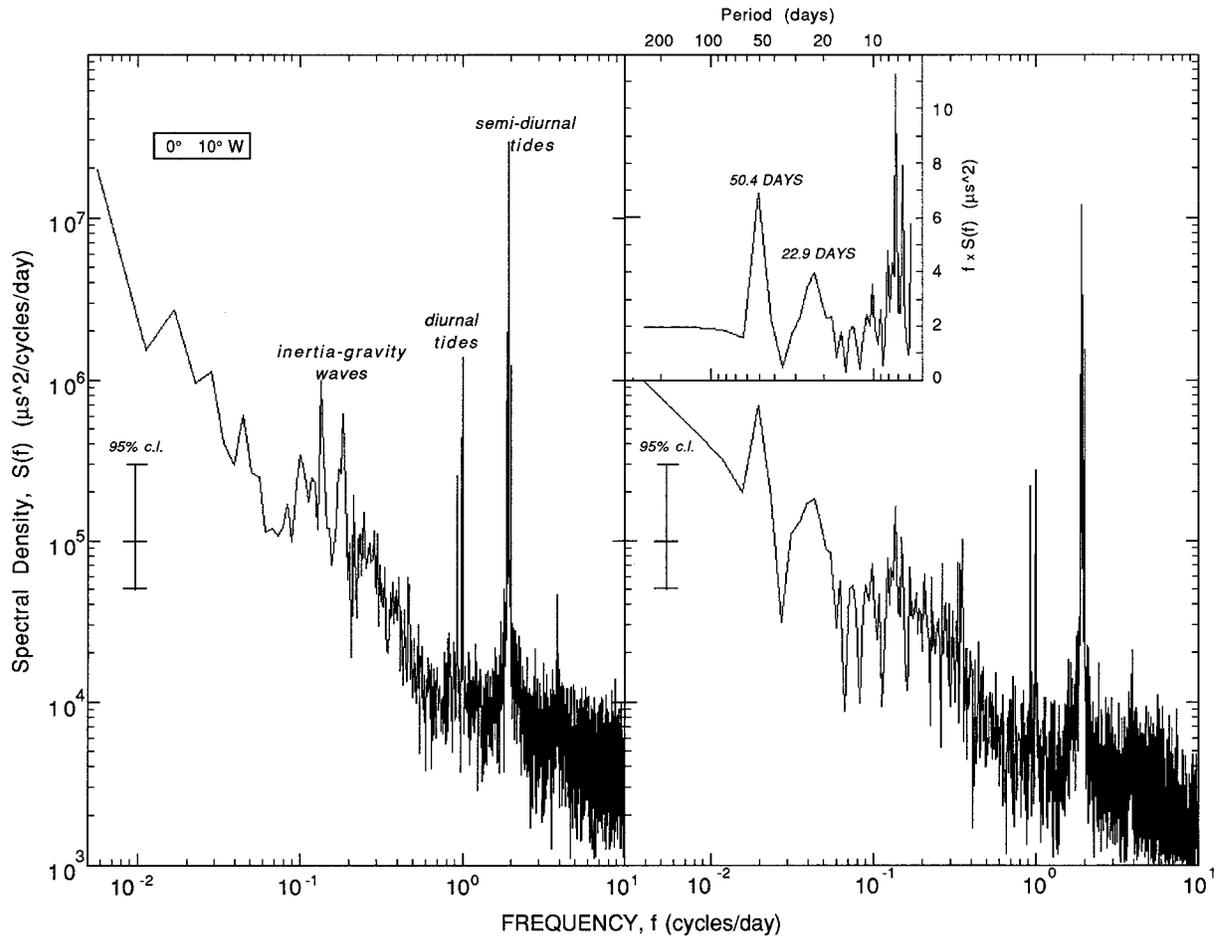
FIG. 2. Energy density spectra of acoustic two-way travel time from the inverted echo sounders. The left panel is from a single sounder averaged over five adjacent raw periodogram values. The major features are identified and the 95% confidence limits shown. The right panel is an average of the five sounders for each frequency band resolved during their common observation period. The insert shows the low frequency end of the spectrum replotted in variance preserving coordinates (frequency times spectral density vs log of frequency).

3. Kelvin wave

a. Sounder

In the 30–60-day band, the gravest function from the CEOF analysis accounts for 81% of the variance in the band. Further discussion is restricted to this first mode, and its time series is shown in Fig. 5. It describes a monotonic, nearly linear, progression in phase with the one minor deviation from linearity occurring when the amplitude is down by a factor of 10. Almost four complete wave cycles are captured in the time interval of 200+ days. Excluding the second cycle, when the signal was weakest, the other three give a best estimate of the wave period as 54 $\pm$ 3 days. This determination of frequency, as well as the picture of just how stable it is, was unobtainable by the earlier method of analysis.

To determine the phase speed, the relative phase of the load factor at each longitude is also plotted in Fig. 5. The difference in phase lag from 34° to 1°W is 2.35 rad, giving a wavelength of 88.4° of longitude (a little larger than the

basin width of 60°). With the wave period of 54 days, this yields a phase speed of 2.11 m s^{-1}, a value 10% less than the 2.35 m s^{-1} computed from Fig. 1. The equivalent depth for a reduced-gravity shallow water wave is 45 cm, a number consistent with theoretical calculations of the first baroclinic mode of an eastward propagating Kelvin wave from averaged oceanographic data describing the vertical profile of density in the equatorial water column.

Also shown in Fig. 5 is the zonal variation of the relative amplitude of the load factor. It does not indicate a statistically significant variation of amplitude with longitude.

b. Altimeter

The raw time series of the first CEOF mode (40% of variance accounted for) is shown in the upper panel of Fig. 6, and the low sampling density (5–6 times per wave cycle) understandably results in a ragged vector diagram. Nevertheless, the rotation and amplitude variation is apparent and, to illustrate it better, the data were interpolated
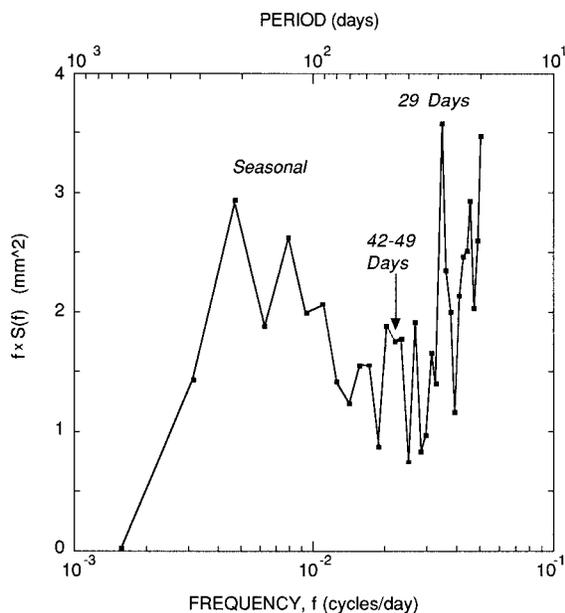
FIG. 3. Variance preserving plot of the altimeter-derived sea surface height. The spectral density is the average of 30 crossings of the equator between 2° and 43°W.

to a daily value (shown in the middle and lower panels). Eighteen wave cycles are observed in the 85 data cycles remaining after the end point tapering employed in the CEOF analysis.

Comparing the amplitude pattern with that from the

sounders, the latter showed one period of signal dropout (January 1985) in the less-than-one-year record. The longer altimeter record suggests an annual signal fading occurring early each year (May 1993, Feb 1994, and Apr 1995) with an additional fading in October 1994. The period of the wave (obtained from the slope of the phase lines in the bottom panel) is constant when the signal is relatively strong and, from an analysis of five time intervals when the phase progression is linear for more than a full rotation, the slopes describe a range of wave periods from 39 to 60 days with a mean of 49.4 days. (This mean will be used in the subsequent calculations.) The wide range can be ascribed either to changes in the forcing or to the seasonal change of mean thermocline depth along the equator.

The load factors of the mode (amplitude and phase) are shown in Fig. 7. The former, shown in the lower panel, suggests a modest increase (20%) of amplitude across the basin, which the sounders did not resolve.

The phase information resulting from the analysis needed to be interpreted before analyzing for wave speed. The first step in the interpretation can be anticipated. Since each pass occurs at a different time of the cycle, during the 10-day altimeter cycle a wave with a 50-day period will be shifted as much as $2\pi \times (10/50)$, or 72° of phase. The sign of the shift depends on whether the site is upstream or downstream of the reference site (20°W from the CEOF analysis, the longitude of maximum variance accounted for by the empirical mode) and whether the pass crossed the equator (in time) before or after the pass
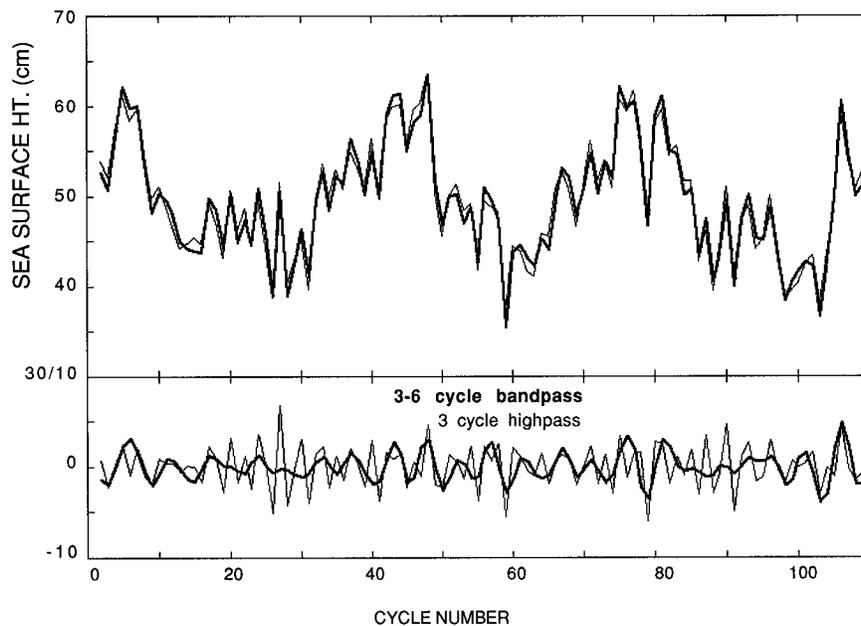

FIG. 4. Sea surface height variation of a typical altimeter equator crossing. Data from pass 87 crossing the equator at 38°W. In the upper panel, the data are shown after processing as described in the text (thin line) and with the additional step of subtracting in-phase variations at 62.1075^{-1} and 11.7994^{-1} cycles day^{-1} (thick line), which could have arisen from an aliasing of the large amplitude M_2 tide.
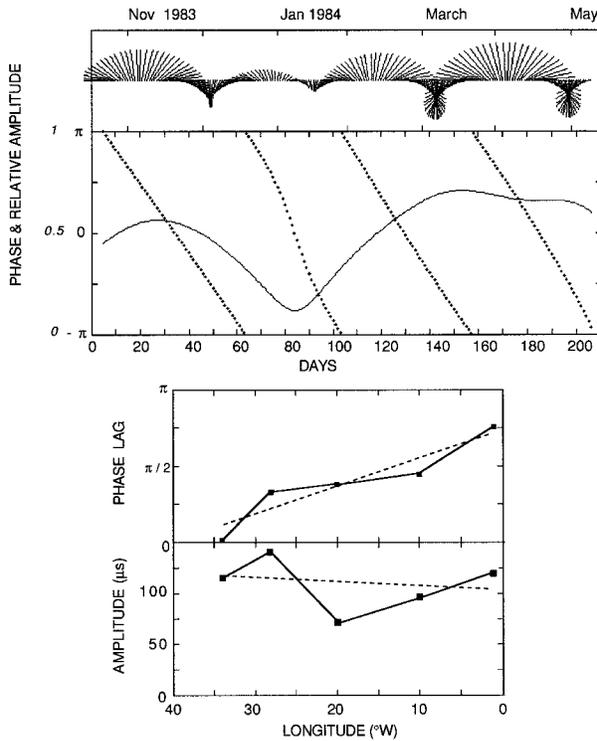
FIG. 5. The first CEOF mode of the sounder data bandpass filtered between 30 and 60 days. The time series (upper panel) shown both as vectors and, for the same data, as a time series of amplitude and phase; and the load factors (lower panel), amplitude and phase, as a function of longitude. The dashed lines are the linear regression of the data with longitude.

over the reference site. After making this adjustment, the phase was plotted as ×'s in the upper panel of Fig. 7. The results show subregions of increasing phase eastward but no overall trend. This is corrected (the second step) by noting that the CEOF analysis is biased to correlating each time series with the smallest possible phase difference. The result is that, to the west of 26°W, it almost always reported the correlation with the next cycle of the wave and, to the east of 13°W, it almost always reported the correlation with the previous cycle. This is corrected by adjusting the regions by $n \times 72°$ ($n = 0$, ± 1, and occasionally ± 2) and the result is shown as squares in Fig. 7. The resulting phase change with longitude, from the linear regression shown on the figure, is 0.0915 radians per degree of longitude, which translates into a basinwide wavelength of 68.6° long and an average wave speed of 1.79 m s^{-1} The similarity to the sounder result (Fig. 5) is emphasized by plotting the sounder-derived rate of phase change through the altimeter data points (dashed line). While the calculated wave speed is slower than the sounder records suggested, variations are expected due to changes in the upper-ocean-layer density field both seasonal and interannual.

4. Tropical instability wave

a. Sampling considerations

As noted in the introduction, the wavelength and period of the TIW is expected to be about ten degrees of longitude and three weeks. Thus the sounder array provides a poor spatial sample and the altimeter a poor temporal sample. Indeed, it would be impossible to un-
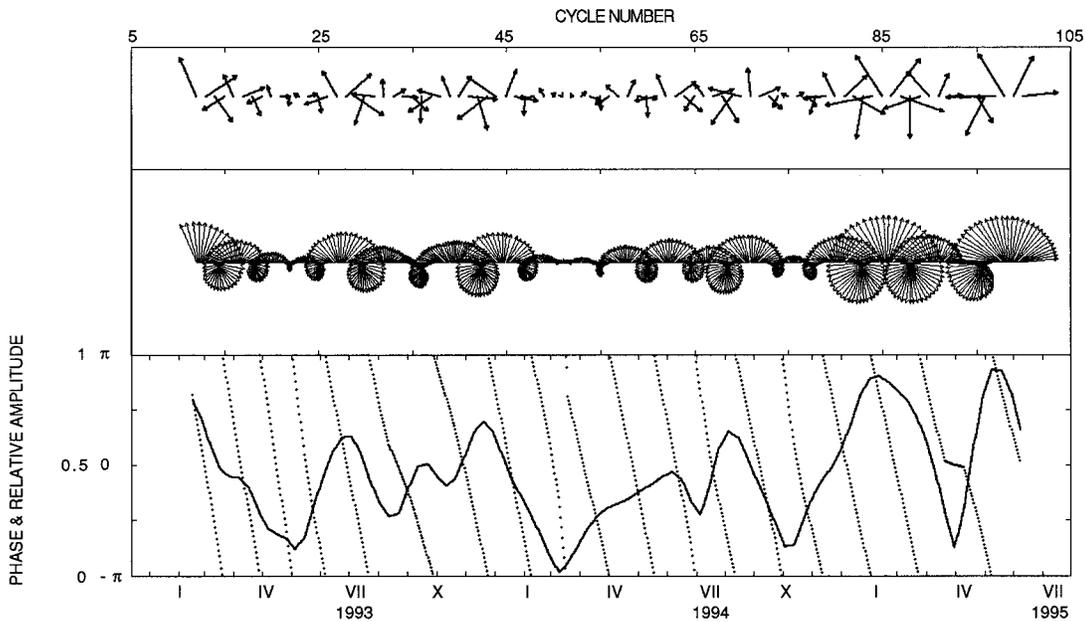

FIG. 6. The first CEOF mode of the altimeter data bandpass filtered between 3 and 6 cycles. Upper diagram is the time series plotted at the resolution of the data and below are linear interpolations of that data to daily values shown in a manner equivalent to the sounder analysis (previous figure).
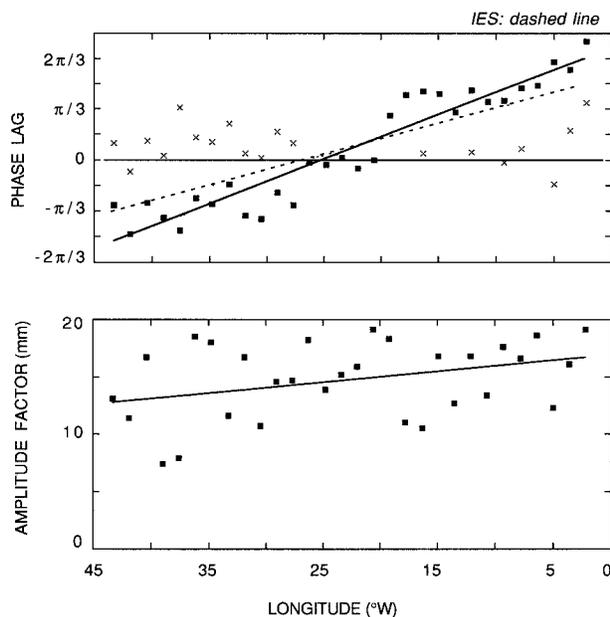
FIG. 7. The load factors (amplitude and phase) of the altimeter data bandpass filtered between 3 and 6 cycles. In the upper panel, the ×'s record the result of the analysis after correcting for relative time of each pass within the cycle while the squares are after the second adjustment (integer increments of 72°, as explained in the text). The linear regression of the adjusted data on longitude is shown as a solid line and is compared to the sounder regression (dashed line) in the upper panel.

ambiguously obtain the wavelength from the sounder array (though it gives a much better picture of the time series rotation) and therefore the altimeter analysis is presented first.

In both CEOF analyses, a problem arose in the higher frequency band because the center frequencies of the two energetic bands are a factor of 2 apart. Thus, noise in the Kelvin wave frequency band showed up as a spurious signal in the TIW frequency band and given the relative amplitude between the two signals, it dominated the CEOF analysis and showed up as the gravest mode (nearly half of the variance). It was however found that the second CEOF (26% of the variance from the five sounders and 12% of the variance from the 30 altimeter crossings of the equator) described the TIW and the results described below are of this second CEOF mode.

b. Altimeter

The time series of the CEOF mode is shown in Fig. 8. During the 872.6 days of filtered data, there are 30.9 rotations of the vector, yielding a wave period of 28.25 days. While there are periods of increased amplitude, no clear seasonal pattern is discerned. The phase change with longitude of the amplitude factor is shown in Fig. 9, first as ×'s, which are only corrected for the relative time of sampling and then as boxes with multiples of 2π added to produce a linear change ($R^2 = .997$) across the basin. The resulting regression is -1.23 radians of phase lag per degree of longitude or a westward propagating wave of wavelength 5.11° long (570 km). The speed of propagation is therefore -23 cm s^{-1}.

The amplitude variation with longitude (Fig. 9) is not monotonic, but a linear regression (solid line) suggests a 30% decrease downstream to the west.

c. Sounders

The time series of the second mode from the CEOF analysis is shown in Fig. 10 and the daily sampling is now sufficient to show the rotation clearly. As with the
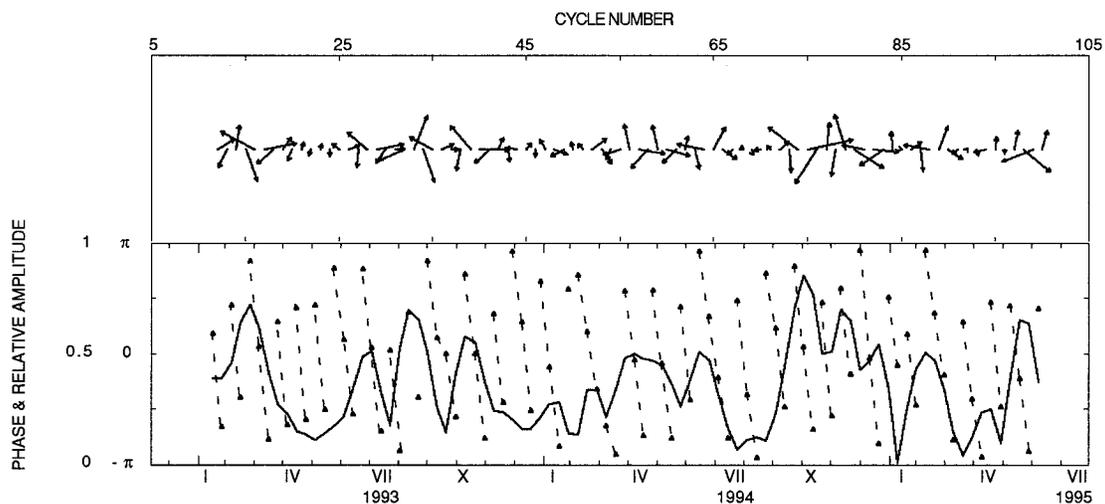

FIG. 8. Time series of the second CEOF mode of the altimeter data high-pass filtered at 3 cycles. Data are plotted once per cycle. The phase angle, shown as triangles in the lower panel, are connected by dashed lines to show the phase progression despite the poor sampling.
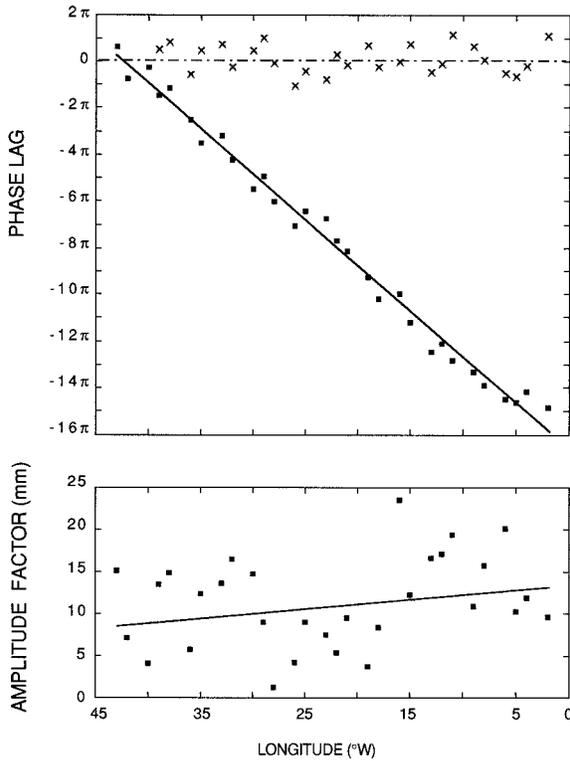
FIG. 9. The load factors (amplitude and phase) of the mode shown in Fig. 8. The analysis values of phase are shown as ×'s in the upper panel, corrected for time of observation within the cycle. The squares are these values after montonically decreasing the lag to the east by factors of 2. On average, an additional 2π is subtracted every 5° of longitude. The linear regressions are also shown.

altimeter data there is no discernible seasonal pattern in the amplitude. A little more than eight wave cycles are depicted and they yield a period of 23.5 days. Figure 11 is the counterpart of Fig. 9 and the results are a very comparable wavelength of 5.45° long (610 km) and a westward phase speed of −30 cm s⁻¹. Once again there is a hint (though not statistically significant) of decreasing amplitude downstream.
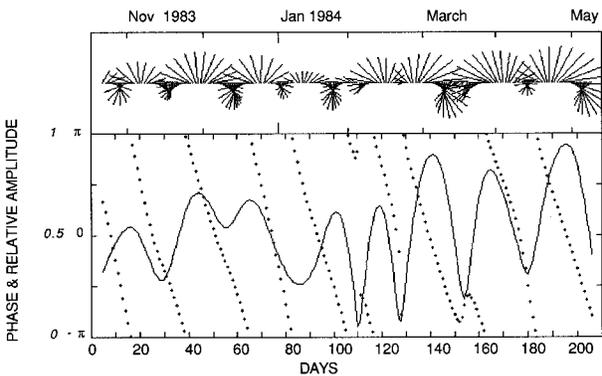

FIG. 10. Time series of the second CEOF mode of the sounder data bandpass filtered between 10 and 30 days.
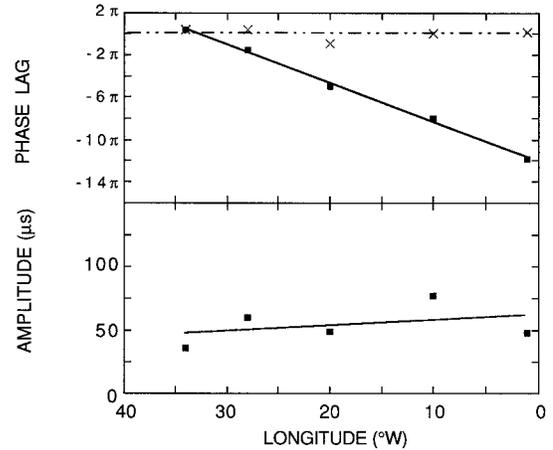

FIG. 11. The load factors (amplitude and phase) of the mode shown in Fig. 10. The phase lag (×'s) are displaced by factors of 2π and the linear regression of both on longitude are shown by solid lines.

5. Discussion

a. Summary

Two entirely different ways of measuring/inferring the temporal variations of sea surface height along the equator, and observations made at two time periods separated by ten years, exhibit enhanced variance in the same two sub-semiannual frequency bands. The variance is explained as eastward/westward wave propagation with qualitatively similar characteristics, coherent across the basin with little or no change in amplitude. Quantitatively, the following was found:

	Kelvin wave		TIW	
	IES	T/P	IES	T/P
average period (days)	54	49.4	23.5	28.25
wave speed (m s⁻¹)	2.11	1.79	−0.30	−0.23
wavelength (10³ km)	9.8	7.6	0.605	0.57

Some of the above differences may be attributable to a change in the ocean between the two observations (i.e., natural variation) and some to the method of observation, the length of time being averaged over, and the uncertainty in the estimates themselves. With regard to the TIW, one might reasonably expect the wave period to be more accurately described by the sounders and the wavelength by the altimeter; thus a best estimate of the wave speed (combining the measurements and ignoring possible interannual differences) would be −0.28 m s⁻¹.

b. Kelvin wave

The lower frequency wave, on the basis of its wave speed range corresponding to theoretical calculations, is identified as a first baroclinic Kelvin wave. It is be-

lieved to be the result of changes in the westward wind stress (e.g., Philander 1990, p. 143) and a wave packet traveling at a Kelvin wave speed has been identified in the Pacific as initiated by a change in the zonal wind stress in the west (Knox and Halpern 1982). Indeed, the zonal wind speed from an in situ wind recorder deployed on St. Peter and Paul Rocks (1°N, 29°W) was shown to correlate with the sounder data (Katz 1987a).

In the absence of any in situ winds to compare with the altimeter observations, it is not possible to examine in any detail how the integrated wind field results in the continuous modulation of the Kelvin wave amplitude shown in Fig. 6. However, large-scale models of the wind during the time of the observations are available, and the seasonal variation of wave amplitude can be compared to a model description of the seasonal wind field.

For this limited purpose, a three-week weighted average of the zonal wind stress at the sea surface was computed from the weekly gridded averages of the National Meteorological Center (now known as the National Centers for Environmental Prediction) model (T-62). It was then averaged in the region 2°N and S, 36°–40°W, to describe the wind forcing in the west where it is largest and presumably initializes the Kelvin wave propagation. These waves will be modified by the continual forcing across the basin [as discussed by Weisberg and Tang (1990) and others], and thus examining the wind field only in the west does not allow for examining the downstream variation in wave amplitude. However, since the analysis of the altimeter data extracted only the part of the wave field that is coherent across the basin, the comparison with the wind stress in the west is self-consistent. Likewise, any westward traveling Rossby waves that may be in the data are excluded by the analysis.

Qualitatively, the relationship between wind changes and wave amplitude is noted in Fig. 12, which compares the time-dependent amplitude of the first CEOF mode (redrawn from Fig. 6) with the derived equatorial wind stress. The four interior peaks of wave amplitude (free of end effects of the analysis) are tracked down to the wind record by the broken lines. The boreal summer peaks (beginning of July) are seen to occur near the end of the sustained annual increase of trade winds (beginning in May), while the boreal winter peaks (particularly in January 1995) occur one month after the annual cessation of the trades. Periods of relatively constant wind stress (high or low) are seen to be cotemporal with minima in wave amplitude.

c. The tropical instability wave

The earliest sustained measurement of the Atlantic Equatorial Undercurrent (Rinkel 1969) reported a 2–3-week meridional oscillation of the current in the Gulf of Guinea. Subsequent observations of the core of the current at various longitudes (defined by either the zonal
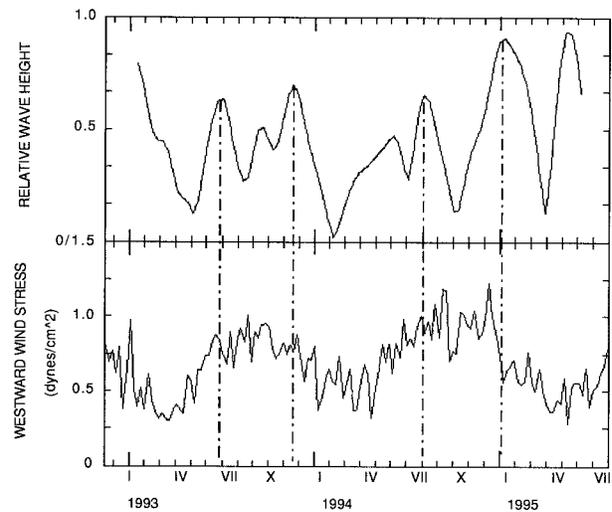

FIG. 12. Kelvin wave amplitude (Fig. 6) compared to zonal wind stress along the equator in the western Atlantic. Source and processing of wind data is described in the text.

current or salinity maxima) suggest an oscillation within the limits of one degree north and south of the equator (e.g., Düing et al. 1975; Katz et al. 1979). This movement can be expected to produce a surface height signal of the small amplitude shown in Fig. 4, as can be inferred from the short-scale zonal variations in dynamic height in the classic International Geophysical Year (1958) R/V *Crawford* equatorial section [Figure 5 of Katz et al. (1977)].

Comparing the present results with the aforementioned summary by Qiao and Weisberg (1995), there is a general consensus independent of the method of measurement that there are westward propagating waves with a period of 20–25 days in the equator and near-equatorial region. Most compute a wavelength of about 1000 km, as did Legekis and Reverdin (1987) from satellite-derived SST observations in the Atlantic; so the present estimate of 600 km is on the low side of previously reported values and this carries over to the calculation of wave speed (values are typically twice that reported here).

Finally, there is some disagreement as to the longitudinal coherency of the TIW. From current meter moorings in the Atlantic, Weisberg and Weingartner (1988) found them to be coherent across a 3000-km mooring array (24°), while from moorings in the Pacific, Halpern et al. (1988) reported the lack of statistically significant horizontal coherence between moorings 15° apart along the equator at the frequency of 0.05 cycles day^{-1}. The present analysis in the Atlantic agrees with the former results.

REFERENCES

Benanda, R., 1993: PO. DAAC merged GDR (TOPEX/Poseidon) users' handbook. Version 1.0, JPL Publ. D-11007; 84 pp.

Cartwright, D. E., 1982: The tidal signal in inverted echo-sounder records. *Deep-Sea Res.,* **29A,** 767–784.

Düing, W., P. Hisard, E. J. Katz, J. Knauss, J. Meincke, K. V. Moroshkin, G. Philander, A. Rybnikov, S. Thorpe, and K. Voight, 1975: Meanders and long waves in the equatorial Atlantic. *Nature,* **257,** 280–284.

Garzoli, S. L., and E. J. Katz, 1981: Observations of inertia-gravity waves in the Atlantic from inverted echo sounders during FGGE. *J. Phys. Oceanogr.,* **11,** 1463–1477.

Halpern, D., R. A. Knox, and D. S. Luther, 1988: Observations of 20-day period meridional current oscillations in the upper ocean along the Pacific equator. *J. Phys. Oceanogr.,* **18,** 1514–1534.

Horel, J. D., 1984: Complex principal component analysis: Theory and examples. *J. Climate Appl. Meteor.,* **23,** 1660–1673.

Katz, E. J., 1987a: Equatorial Kelvin waves in the Atlantic. *J. Geophys. Res.,* **92,** 1894–1898.

——, 1987b: Seasonal response of the sea surface to the wind in the equatorial Atlantic. *J. Geophys. Res.,* **92,** 1885–1893.

——, R. Belevich, J. Bruce, V. Bubnov, J. Cochrane, W. Düing, P. Hisard, H. U. Lass, J. Meincke, A. deMesquita, L. Miller, and A. Rybnikov, 1977: Zonal pressure gradient along the equatorial Atlantic. *J. Mar. Res.,* **35** (2), 293–307.

——, J. G. Bruce, and B. D. Petrie, 1979: Salt and mass flux in the Atlantic Equatorial Undercurrent. *Deep-Sea Res.,* **26,** (G Suppl. II), 137–160.

——, A. Busalacchi, M. Bushnell, F. Gonznalez, L. Gourdeau, M. McPhaden, and J. Picaut, 1995: A comparison of coincidental time series of the ocean surface height by satellite altimeter, mooring and inverted echo sounder. *J. Geophys. Res.,* **100,** 25 101–25 108.

Knox, R. A., and D. Halpern, 1982: Long range Kelvin wave propagation of transport variations in Pacific Ocean equatorial currents. *J. Mar. Res.,* **40,** 329–339.

Legeckis, R., 1977: Long waves in the eastern Equatorial Pacific Ocean: A view from a geostationary satellite. *Science,* **197,** 1179–1181.

——, and G. Reverdin, 1987: Long waves in the Equatorial Atlantic Ocean during 1983. *J. Geophys. Res.,* **92,** 2835–2842.

Philander, S. G. H., 1976: Instabilities of zonal equatorial currents. *J. Geophys. Res.,* **81,** 3725–3735.

——, 1981: The response of equatorial oceans to a relaxation of the trade winds. *J. Phys. Oceanogr.,* **11,** 176–189.

——, 1990: *El Niño, La Niña, and the Southern Oscillation.* Academic Press, 289 pp.

Proehl, J. A., 1996: Linear stability of equatorial zonal flows. *J. Phys. Oceanogr.,* **26,** 601–621.

Qiao, L., and R. H. Weisberg, 1995: Tropical instability wave kinematics: Observations from the Tropical Instability Wave Experiment. *J. Geophys. Res.,* **100,** 8677–8692.

Rinkel, M. O., 1969: *Proc. Symp. Oceanography Fish. Resources Tropical Atlantic.* UNESCO, Paris, France, 193–212.

Weisberg, R. H., and T. Y. Tang, 1987: Further studies on the response of the equatorial thermocline in the Atlantic Ocean to the seasonally varying trade winds. *J. Geophys. Res.,* **92,** 3709–3727.

——, and T. J. Weingartner, 1988: Instability waves in the equatorial Atlantic Ocean. *J. Phys. Oceanogr.,* **18,** 1641–1657.

——, and T. Y. Tang, 1990: A linear analysis of equatorial Atlantic Ocean thermocline variability. *J. Phys. Oceanogr.,* **20,** 1813–1825.